

Multiproxy reconstructions of integral energy spectra for extreme solar particle events of 7176 BCE, 660 BCE, 775 CE and 994 CE

Sergey Koldobskiy^{1,2}, Florian Mekhaldi^{3,4}, Gennady Kovaltsov¹, Ilya
Usoskin^{1,2}

¹Space Physics and Astronomy Research Unit, University of Oulu, Finland

²Sodankylä Geophysical Observatory, University of Oulu, Finland

³Department of Geology-Quaternary Sciences, Lund University, Lund, Sweden

⁴British Antarctic Survey, Ice Dynamics and Paleoclimate, Cambridge, UK

Key Points:

- Integral fluxes (fluences) of four extreme solar particle events (ESPEs) are reconstructed using a novel multi-proxy approach.
- ESPE fluences are shown to have a spectral shape similar to the most powerful modern solar particle events but orders of magnitude greater.
- For the reconstruction, we used recent cosmogenic isotope measurements combined with state-of-the-art modelling.

Corresponding author: Sergey Koldobskiy, sergey.koldobskiy@oulu.fi

Abstract

Extreme solar particle events (ESPEs) are rare and the most potent known processes of solar eruptive activity. During ESPEs, a vast amount of cosmogenic isotopes (CIs) ^{10}Be , ^{36}Cl and ^{14}C can be produced in the Earth's atmosphere and deposited in natural stratified archives. Accordingly, CI measurements in these archives allow us to evaluate particle fluxes during ESPEs. In this work, we present a new method of ESPE fluence (integral flux) reconstruction based on state-of-the-art modeling advances, allowing to fit together different CI data within one model. We represent the ESPE fluence as an ensemble of scaled fluence reconstructions for ground-level enhancement (GLE) events registered by the neutron monitor network since 1956 coupled with satellite and ionospheric measurements data. Reconstructed ESPE fluences appear softer in its spectral shape than earlier estimates, leading to significantly higher estimates of the low-energy ($E < 100$ MeV) fluence. This makes ESPEs even more dangerous for modern technological systems than previously believed. Reconstructed ESPE fluences are fitted with a modified Band function, which eases the use of obtained results in different applications.

1 Introduction

The only quantitative way to study solar and the related cosmic-ray variabilities over long timescales beyond the era of direct measurements is through cosmogenic isotopes (CIs, see, *e.g.*, Beer et al., 2012; Usoskin, 2017) which are produced in the Earth's atmosphere by cosmic rays and then are stored in natural independently dateable stratified archives (tree rings, ice cores, sediments, etc.) from where they can be extracted and measured in modern laboratories (*e.g.*, Vonmoos et al., 2006; Brehm et al., 2021). The most important CIs for solar and cosmic-ray studies are ^{14}C (aka radiocarbon) measured in dendrochronologically dated tree rings, as well as ^{10}Be and ^{36}Cl , both measured in glaciologically dated polar ice cores. These cosmogenic isotopes are normally produced by an omnipresent but variable flux of galactic cosmic rays (GCRs), forming the main proxy dataset for long-term solar-activity reconstructions (*e.g.*, Bard et al., 2000; Solanki et al., 2004; Muscheler et al., 2007; Steinhilber et al., 2012; Wu et al., 2018; Usoskin et al., 2021). Sporadic solar energetic particle (SEP) events usually cannot produce a detectable amount of cosmogenic isotopes (Usoskin, Solanki, Kovaltsov, et al., 2006; Usoskin, Koldobskiy, Kovaltsov, Rozanov, et al., 2020; Mekhaldi et al., 2021), but very seldom, roughly once per millennium, extremely strong solar particle events (called ESPEs henceforth) take place, with the SEP event-integrated flux (fluence) exceeding that of 'usual' SEP events by several orders of magnitude (*e.g.*, Cliver et al., 2022). Such events can lead to significant spikes in the cosmogenic-isotope production that can be detected by accelerator mass spectrometry, AMS (*e.g.*, Synal & Wacker, 2010; Miyake et al., 2019). The first such spike, dated to 775 CE, was discovered in 2012 by Miyake et al. (2012) and soon was confirmed to be an ESPE (Usoskin et al., 2013). Since then, four more ESPEs have been confirmed (*i.e.*, independently found in several sources), dated to 994 CE, 660 BCE, 5259 BCE and 7176 BCE (Miyake et al., 2013; Park et al., 2017; O'Hare et al., 2019; Brehm et al., 2022; Paleari et al., 2022). In addition, three ESPE candidates, in 5410 BCE, 1052 CE and 1279 CE (Miyake et al., 2021; Brehm et al., 2022) are waiting for independent confirmation.

Since ESPEs form a type of extremely strong solar eruptive events never observed directly with scientific instrumentation, and may represent new, presently unknown, physical processes on the Sun (Usoskin & Kovaltsov, 2021), it is crucially important to assess their characteristic parameters, specifically, the energy spectrum. Generally, the event-integrated spectrum can be estimated based on data from different isotopes for the same event: ^{14}C and ^{10}Be isotopes are effectively sensitive to SEP with the energy above 230 MeV while the effective energy of SEPs producing ^{36}Cl is much lower, about 60 MeV (Koldobskiy et al., 2022). Recently, several approaches have been used to evaluate the

spectra of the ESPEs. The spectra of the ESPEs of 775 CE and 994 CE (Mekhaldi et al., 2015) as well as around 660 BCE (O’Hare et al., 2019) were estimated by using the relationship between the $^{36}\text{Cl}/^{10}\text{Be}$ ratio and SEP spectral hardness of SEP-induced ground level enhancements (GLEs) registered by ground-based neutron monitor (NM) network (Usoskin, Koldobskiy, Kovaltsov, Gil, et al., 2020). In both studies, the measured ^{10}Be and ^{36}Cl concentrations from Greenland ice cores were compared with modeled production rates induced by modern GLEs, using their spectra and CI production function estimated by Webber et al. (2007). The modern GLE yielding the closest $^{36}\text{Cl}/^{10}\text{Be}$ ratio to those measured for the ESPEs was selected and scaled up by using the prescribed, nearly power-law spectral shape form (Webber et al., 2007), leading to very hard energy spectra. Later, Usoskin, Koldobskiy, Kovaltsov, Rozanov, et al. (2020) postulated that the energy spectrum of the ESPE of 775 CE can be represented by a scaled spectrum of the strongest directly observed hard-spectrum SEP event of 23-Feb-1956 (GLE #5). Similarly to Mekhaldi et al. (2015) and O’Hare et al. (2019), Paleari et al. (2022) leveraged the $^{36}\text{Cl}/^{10}\text{Be}$ ratio from the ice-core measurements during the 7176 BCE ESPE to infer the spectral hardness. However, they did so by combining recent production functions (Poluianov et al., 2016) and GLE spectral fluence reconstructions (Raukunen et al., 2018; Koldobskiy et al., 2021), so that the reconstructed spectrum resulted from an ensemble of modern GLE events. Their reconstructed ESPE spectrum appears softer than those assessed earlier (Mekhaldi et al., 2015; O’Hare et al., 2019) and close to that assessed by Usoskin, Koldobskiy, Kovaltsov, Rozanov, et al. (2020).

Here we develop this approach further and present a systematic reconstruction of integral fluences (event-integrated fluxes) for four ESPEs: 994 CE, 775 CE, 660 BCE and 7176 BCE, using a newly developed method based on a simultaneous fit of the spectral shape to the measured data of all the three cosmogenic isotopes.

2 Data sources

Here we use two data sources related to SEP events: cosmogenic-isotope data for ESPEs during the past millennia, and direct observations of SEP events during the recent decades by spacecraft and NMs – GLEs.

2.1 Cosmogenic isotope data

Here we used data of cosmogenic isotopes ^{10}Be , ^{14}C and ^{36}Cl published for four ESPEs of 7176 BCE, 660 BCE, 775 CE and 994 CE (the dates here are related to the year of the isotope concentration peaks, while the ESPEs could have occurred in the previous calendar year). Details and references to the data are given in Table 1. We carefully selected the data using the recent (re-)estimates, *e.g.*, for ^{10}Be measured for ESPE 775 CE we used reanalysis from Mekhaldi et al. (2021) which supersedes that of Mekhaldi et al. (2015). The isotope production by SEPs during an ESPE is quantified as the global production for ^{14}C and polar deposition flux for ^{10}Be and ^{36}Cl , using the parameterization of atmospheric transport and deposition (Heikkilä et al., 2009, 2013).

The isotope production due to ESPE, Q_{ESPE} , can be inferred from measurement data as an excess of the production rate Q above the background due to GCR, Q_{GCR} . Ideally, from the values of Q_{ESPE} , one could directly estimate the parameters of SEPs. This works well for ^{14}C which is globally mixed and whose production is modelled precisely (Kovaltsov et al., 2012). However, ^{10}Be and ^{36}Cl are subjected to a complicated transport and deposition (Field et al., 2006; Heikkilä et al., 2013; Golubenko et al., 2021) dominated by the local/regional effects on short time scales (Pedro et al., 2006; Usoskin et al., 2009; Zheng et al., 2020). Because of that, there is an unknown scaling factor κ , typically ranging from 0.8–1.3 between the modelled and measured production/deposition rates, related to the local/regional depositional factors (Sukhodolov et al., 2017). This κ -factor is a free parameter and cannot be found from the data alone. Because of this,

Table 1. Data and corresponding geomagnetic/heliospheric conditions for the ESPEs (represented by horizontal blocks) considered in this work. Columns M_K and M_P represent VADM reconstructions, for the time of the events, by Knudsen et al. (2008) and Panovska et al. (2018), respectively, in units of $10^{22} \text{ A}\cdot\text{m}^2$. ϕ is solar modulation potential (see text). ‘Data’ column specifies the data sources: M15 – Mekhaldi et al. (2015), B18 – Büntgen et al. (2018), O19 – O’Hare et al. (2019), the average of NGRIP and GRIP dataset was used, S20 – Sakurai et al. (2020), M21 – Mekhaldi et al. (2021), P22 – Paleari et al. (2022), B22 – Brehm et al. (2022). ‘Type’ represents the type of data (see text for details), viz., P – P peak ratio, and Q – production (in units of 10^8 cm^{-2}). Values of Q were converted to P for the ESPE fluence reconstruction procedure as described in Section 2.1.

Event	M_K	M_P	ϕ , MV	Data	Type	^{10}Be	^{36}Cl	^{14}C
994 CE	10.3 ± 0.4	9 ± 0.5	410 ± 100	M15	P	1.2 ± 0.2	2.6 ± 0.3	2.40 ± 0.70
				B18	P			1.80 ± 0.40
				B18	Q			1.04 ± 0.10
				B22	Q			1.18 ± 0.10
775 CE	10.7 ± 0.4	9.3 ± 0.5	525 ± 100	M15	P		6.3 ± 0.4	3.90 ± 0.70
				B18	P			3.20 ± 0.20
				B18	Q			1.88 ± 0.10
				M21	P	3.0 ± 0.2		
				B22	Q			2.21 ± 0.10
660 BCE	11.4 ± 0.6	9 ± 0.4	390 ± 100	O19	P	3.8 ± 1.3	6.4 ± 1.4	
				S20	Q			1.40 ± 0.10
				B22	Q	2.5 ± 0.9		1.62 ± 0.2
				P22	P			
7176 BCE	8.7 ± 1.7	7.5 ± 0.4	550 ± 100	P22	P	3.7 ± 0.4	6.1 ± 1.2	4.50 ± 0.50
				B22	Q			2.42 ± 0.1

a conversion between the production rate and the SEP spectrum becomes uncertain at a $\pm 20\%$ level. To avoid that, the so-called peak factor P is often used as an index of the ESPE strength (*e.g.*, Mekhaldi et al., 2015) that is the ratio of the measured isotope’s production/deposition excess Q_{ESPE} to the background annual isotope’s production/deposition rate Q_{GCR} before and after the ESPE:

$$P_{\text{ESPE}} = Q_{\text{ESPE}}/Q_{\text{GCR}}. \quad (1)$$

Under the assumption that the k -factor is the same for SEP- and GCR-produced isotope atoms, the P ratio appears free of the k -factor eliminating the related uncertainty. Additionally, a ratio between background concentration and peak concentration can be used for the same purpose, neglecting uncertainties of translation from measured concentration to deposition flux. Accordingly, we used the measured ratio P for ^{10}Be and ^{36}Cl as a quantitative index of the ESPE strength, in this work. For ^{14}C , if Q_{ESPE} -values were published, we converted them to the P -values using equation 1.

Table 2. List of GLE events considered here.

GLE(s)	Date	GLE(s)	Date
5	23/02/1956	38	07/12/1982
8	04/05/1960	39	16/02/1984
10–12	Nov. 1960	40	25/07/1989
13	18/07/1961	41	15/08/1989
16	28/01/1967	42–45	Oct.–Nov. 1989
18	29/09/1968	46	15/11/1989
19	18/11/1968	47–50	May1990
20	25/02/1969	51–52	Jun1990
21	30/03/1969	53	25/06/1992
22	24/01/1971	55	06/11/1997
23	01/09/1971	56	02/05/1998
24–25	Aug. 1972	58	24/08/1998
26	29/04/1973	59	14/07/2000
27	30/04/1976	60–61	Apr. 2001
28–29	Sep. 1977	62	04/11/2001
30	22/11/1977	63	26/12/2001
31	07/05/1978	64	24/08/2002
32	23/09/1978	65–67	Oct.–Nov. 2003
33	21/08/1979	69	20/01/2005
35	10/05/1981	70	13/12/2006
36	12/10/1981	71	16/05/2012
37	26/11/1982	72	10/09/2017

2.2 Direct data: ground-level enhancements since 1956

Thousands of SEP events, including weak ones, have been directly measured *in situ* by spacecraft during the recent decades (Vainio et al., 2013; Desai & Giacalone, 2016), but only several tens of them were sufficiently strong and energetic to initiate a nucleonic cascade in the Earth’s atmosphere and thus potentially produce cosmogenic isotopes. However, the directly observed SEP events for the last 70 years were unable to produce a detectable amount of CIs (Usoskin, Koldobskiy, Kovaltsov, Gil, et al., 2020; Mekhaldi et al., 2021). Strongest SEP events were registered by ground-based neutrons monitors (NMs) as GLE events (Usoskin, Koldobskiy, Kovaltsov, Gil, et al., 2020) that serve as reference events for ESPes (Usoskin, Koldobskiy, Kovaltsov, Rozanov, et al., 2020; Mekhaldi et al., 2021). SEP spectral fluences (event- and energy-integrated fluxes) from ~ 30 MeV to several GeVs have been recently reconstructed for 58 moderate and strong GLE events by Koldobskiy et al. (2021) based on a combination of ground-based and space-borne datasets. Here we used these spectral reconstructions as an ensemble of reference spectra, similarly to Mekhaldi et al. (2021) and Paleari et al. (2022).

The highest typically achievable time resolution for paleo-events (including ESPes) is of one year, or seasonal at best. Considering also the residence time of CI in the atmosphere (less than one year for ^{14}C (Beer et al., 2012), 1–2 years for ^{10}Be and ^{36}Cl (Heikkilä et al., 2009)), the CI method cannot distinguish between a single extreme event and a series of consequent events as, e.g., in October–November 1989. Accordingly, for further analysis, we have combined ‘serial’ GLEs produced by the same solar active region into pseudo-single GLE events with the summed spectral fluences. The list of the considered GLEs (single and serial) is given in Table 2.

For each GLE event, the integral omnidirectional fluence F (in units of cm^{-2}) was parameterized over rigidity R with the modified Band function (MBF), which is a dou-

ble power-law with an exponential roll-off (Koldobskiy et al., 2021):

$$\begin{aligned} F(> R) &= J_1 \left(\frac{R}{1 \text{ GV}} \right)^{-\gamma_1} \exp \left(-\frac{R}{R_1} \right) \quad \text{if } R < R_b, \\ F(> R) &= J_2 \left(\frac{R}{1 \text{ GV}} \right)^{-\gamma_2} \exp \left(-\frac{R}{R_2} \right) \quad \text{if } R \geq R_b, \end{aligned} \quad (2)$$

where $\gamma_1, R_1, J_1, \gamma_2, R_2$ are parameters of the fit and R is the SEP rigidity in GV. Parameters γ_0, R_b and J_1 can be calculated using other parameters:

$$\begin{aligned} \gamma_0 &= \gamma_2 - \gamma_1 \\ R_0 &= R_1 \cdot R_2 / (R_2 - R_1) \\ R_b &= \gamma_0 \cdot R_0 \\ J_1 &= J_2 \cdot R_b^{-\gamma_0} \cdot \exp(\gamma_0). \end{aligned} \quad (3)$$

The MBF can be analytically differentiated yielding the differential flux of SEPs over rigidity $dF/(dR d\Omega) \equiv J$ (in units of $\text{cm}^{-2}\text{GV}^{-1}\text{sr}^{-1}$) assuming the isotropic SEP flux:

$$\begin{aligned} J(R) &= \frac{1}{4\pi} J_1 \left(\frac{R}{1 \text{ GV}} \right)^{-\gamma_1} \exp \left(-\frac{R}{R_1} \right) \left(\frac{\gamma_1}{R} + \frac{1}{R_1} \right) \quad \text{if } R < R_b, \\ J(R) &= \frac{1}{4\pi} J_2 \left(\frac{R}{1 \text{ GV}} \right)^{-\gamma_2} \exp \left(-\frac{R}{R_2} \right) \left(\frac{\gamma_2}{R} + \frac{1}{R_2} \right) \quad \text{if } R \geq R_b, \end{aligned} \quad (4)$$

These differential fluxes are used for computations of the cosmogenic isotope production as described in Sect. 2.3.

2.3 Modelling of production and deposition of cosmogenic isotopes

For a comparison with the measured data, we computed the modelled production of cosmogenic isotopes in the Earth's atmosphere using the approach based on the yield functions (Poluianov et al., 2016). This allowed us to compute the CI production in the atmosphere, but the measured data include also atmospheric transport and deposition. Radiocarbon (^{14}C) is usually taken as globally mixed in the atmosphere and then involved in the global carbon cycle, often modelled by a 'multi-box' model (*e.g.*, Büntgen et al., 2018). For ^{10}Be and ^{36}Cl , the measured quantity is concentration in ice, which is sometimes subsequently translated, via the snow accumulation rate, into the depositional flux which is related to the atmospheric production via transport and deposition processes, accounted for in a parameterized approach by Heikkilä et al. (2009, 2013). To consider these transport/deposition processes, we used the 'effective' yield functions Y_{eff} which account for the global production of ^{14}C and production + transport + polar deposition for ^{10}Be and ^{36}Cl (Asvestari et al., 2017; Koldobskiy et al., 2022).

For the GCR-based production, we modelled the GCR spectrum using the broadly used force-field approximation (*e.g.*, Caballero-Lopez & Moraal, 2004) applying the local interstellar spectrum of GCRs according to Vos and Potgieter (2015), constructed to fit both low-energy data from Voyager satellites at the outer heliospheric boundary and higher-energy data from modern PAMELA and AMS-02 satellites. Heavier ($Z > 1$) nuclei were considered following the approach described in Koldobskiy et al. (2019). The force-field model includes only one variable parameter, the modulation potential ϕ (see the methodology in, *e.g.*, Usoskin et al., 2005). There have been many estimates of the modulation potential in the past (*e.g.*, Vonmoos et al., 2006; Steinhilber et al., 2012) but they are not always inter-comparable because the modulation potential is a slightly model-dependent quantity (Usoskin et al., 2005; Herbst et al., 2010). For consistency, here we use the values of ϕ corresponding to the times of ESPEs as obtained or reconstructed using the same methodology from Usoskin et al. (2021) for ESPE 994 CE, from

Sukhodolov et al. (2017) for 775 CE, and from Wu et al. (2018) for the times of 660 BCE and 7176 BCE. The collected ϕ -values, along with their uncertainties, are presented in column 4 of Table 1.

Since the flux of cosmic rays, both GCRs and SEPs, near Earth is modulated also by the geomagnetic field, whose intensity and directions slowly change in time, it is essential to consider a realistic geomagnetic field during the times of ESPEs. The geomagnetic shielding of charged particles is mostly affected by the dipole component of the geomagnetic field (*e.g.*, Nevalainen et al., 2013) which is often quantified in terms of the virtual dipole moment (VDM) or, typically for paleomagnetic reconstructions, the virtual axial dipole moment (VADM – see. *e.g.*, Usoskin, Solanki, & Korte, 2006), denoted henceforth as M . Here we considered two archeo/paleomagnetic reconstructions, which are independent from CI data and based on different approaches, to assess the geomagnetic shielding during the times of ESPEs, by Knudsen et al. (2008) and by Panovska et al. (2018), the VADM values being denoted as M_K and M_P , respectively, to cover the full range of uncertainties. The collected M -values, along with their uncertainties, are presented in columns 2 and 3 of Table 1.

Using the effective yield functions, the measured quantities of the CIs (Section 2.1) produced by cosmic rays of the given origin (GCR or SEP) can be calculated as:

$$Q(t) = \sum_l \int_0^\infty J_l(R, t) \cdot Y_{\text{eff},l}(R, M(t)) \cdot dR, \quad (5)$$

where the summation is over types of cosmic-ray particles (proton, α -particles, heavier species), $J_l(R, t)$ is the differential rigidity spectrum of the l -th specie at moment t , $Y_{\text{eff},l}(R, M)$ is the effective yield function for the particle of type l , $M(t)$ is the VADM value, and the integration is over the rigidity.

3 Spectral reconstruction

The procedure of the reconstruction of the spectral fluence for individual ESPEs is based on an iterative Monte-Carlo approach as described below in consecutive steps.

1. For a given ESPE, a set of the experimental cosmogenic proxy data along with their uncertainties was selected from Table 1. The data sources were chosen randomly and independently for each isotope (*e.g.*, M21, M15 and B18 could be randomly selected for ^{10}Be , ^{36}Cl and ^{14}C , respectively, for the 775 CE event). In this way, a set of three values of the ESPE peak factors $P_{\text{ESPE},i}$ (index i correspond to different isotopes) and the corresponding uncertainties $\sigma_{\text{ESPE},i}$ were selected.
2. For each GLE (single or 'serial') listed in Table 2, we simulated its differential fluence in the form of MBF (Equation 4), where the exact values of parameters were randomly (with the normally-distributed pseudo-random numbers with zero mean and unity variance) taken from the uncertainty range as reported in Table 2 of Koldobskiy et al. (2021). Accordingly, we obtain a set of SEP differential spectra J_j , where j is the number of individual or 'serial' GLE event as listed in Table 2.
3. For each SEP differential flux J_j , obtained at step 2 above, we calculated the expected ^{14}C global production and deposition fluxes of ^{10}Be and ^{36}Cl , viz. $Q_{i,j}^*$, using Equation 5. The geomagnetic shielding was modelled for each ESPE with the VADM value M^* being simulated using a normally-distributed pseudo-random number r (zero mean, unity variance) as $M^* = M + r \cdot \sigma_M$, where M and σ_M are taken from Table 2. In addition, it was simulated randomly with the equal probability, whether M_K or M_P values are used. The M^* value was taken the same for the calculation of the SEP-induced production/deposition of all three cosmogenic isotopes within one realisation.
4. Next, we calculated the annual global production (for ^{14}C) or deposition fluxes (for ^{10}Be and ^{36}Cl) of CIs due to GCRs, $Q_{\text{GCR},i}^*$, using the M^* values as obtained

Table 3. Reconstructed ESPE fluences in units of cm^{-2} .

ESPE	$F_{30} \cdot 10^{11}$	$F_{60} \cdot 10^{11}$	$F_{100} \cdot 10^{10}$	$F_{200} \cdot 10^{10}$	$F_{300} \cdot 10^9$	$F_{600} \cdot 10^9$	$F_{1000} \cdot 10^8$
994 CE	$1.16^{+0.41}_{-0.53}$	$0.39^{+0.10}_{-0.07}$	$1.72^{+0.32}_{-0.30}$	$0.46^{+0.08}_{-0.07}$	$1.87^{+0.43}_{-0.29}$	$0.33^{+0.07}_{-0.08}$	$0.70^{+0.24}_{-0.24}$
775 CE	$2.87^{+0.84}_{-0.62}$	$1.03^{+0.24}_{-0.15}$	$4.29^{+0.96}_{-0.62}$	$1.04^{+0.21}_{-0.13}$	$3.99^{+1.01}_{-0.44}$	$0.66^{+0.17}_{-0.13}$	$1.32^{+0.65}_{-0.30}$
660 BCE	$2.43^{+1.67}_{-1.08}$	$0.99^{+0.39}_{-0.31}$	$4.42^{+1.08}_{-1.00}$	$1.16^{+0.17}_{-0.14}$	$4.61^{+0.84}_{-0.65}$	$0.79^{+0.21}_{-0.22}$	$1.64^{+0.58}_{-0.65}$
7176 BCE	$1.62^{+0.50}_{-0.72}$	$0.78^{+0.17}_{-0.35}$	$4.01^{+0.88}_{-1.64}$	$1.28^{+0.25}_{-0.29}$	$5.67^{+0.87}_{-0.74}$	$1.05^{+0.45}_{-0.20}$	$2.15^{+2.60}_{-0.47}$

at step 3. The exact value of the modulation potential ϕ^* (column 4 in Table 1) was simulated using a normally distributed pseudo-random number as $\phi^* = \phi + r \cdot \sigma_\phi$. The same value of ϕ^* was used for all isotopes at this step. After that, we calculated the peak factors for each individual or 'serial' GLE event: $P_{i,j}^* = Q_{i,j}^*/Q_{\text{GCR},i}^*$.
 5. For each set of $P_{i,j}^*$ modelled above, we found a scaling factor κ_j which scales the CIs modelled for the j th GLE to match the observed peak factors in CI data. This is quantified via the minimization of the χ^2 merit function:

$$\chi_j^2 = \sum_i \left(\frac{\kappa_j \cdot P_{i,j}^* - P_{\text{ESPE},i}}{\sigma_{\text{ESPE},i}} \right)^2, \quad (6)$$

where $P_{\text{ESPE},i}$ and $\sigma_{\text{ESPE},i}$ are taken at step 1 from columns 7–9 of Table 1, and the summation is over the three cosmogenic isotopes. The best-fit solution of Equation 6 can be found analytically as

$$\kappa_j = \frac{\sum P_{i,j}^* \cdot P_{\text{ESPE},i} / \sigma_{\text{ESPE},i}^2}{\sum (P_{i,j}^* / \sigma_{\text{ESPE},i})^2}. \quad (7)$$

The best-fit scale factors κ_j and the corresponding values of χ_j^2 were saved for each realization.

Steps 1–5 were repeated in 1000 realizations and the corresponding matrices of $\chi_{j,k}^2$, best-fit scaling factors $\kappa_{j,k}$ and MBF parameters were collected, where k denotes the number of the realization. During this iterative process, all pseudo-random numbers used in the simulations were calculated independently and anew at each step and each realization.

Two additional criteria were then applied for each realization to get a reliable solution:

- Only realizations with the best-fit $\kappa \leq 3500$ were selected to exclude amplification of noise. Realizations with $\kappa > 3500$ were discarded.
- Only realizations with $\chi^2 \leq 5.99$ were selected, as corresponding, with two degrees of freedom, to the p -value of 0.05 implying that the considered model fits the data reasonably well (Press et al., 2007).

Realizations passing these selection criteria were used to form an ensemble of 'good fits' of the ESPE integral fluence estimates defined as $F_{\text{ESPE}} = \kappa_j F_{\text{GLE},j}$, where $F_{\text{GLE},j}$ is the integral fluence of the j -th GLE computed using the stored MBF parameters. For this ensemble, the median value and the 68% confidence intervals of F_{ESPE} were calculated for each rigidity, as shown in Figures 1 and 2. Numeric values of reconstructed ESPE fluences $F(> E)$ for selected energies are given in Table 3, and tables with finer energy resolution (10 bins per energy decade) are given as Supplementary Material.

To check the robustness of ESPE fluence estimates, we also consider the effect of systematic change in M and ϕ values used for reconstruction. Change of M by 10% leads

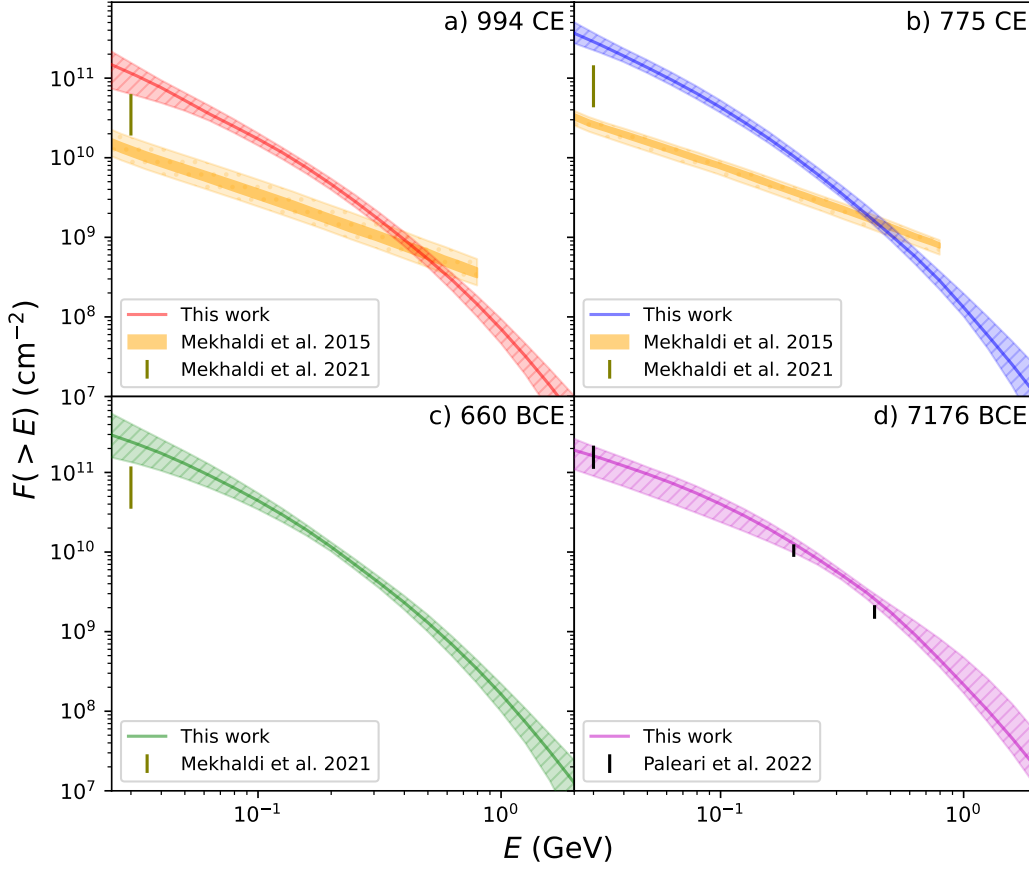


Figure 1. Integral spectral fluences of ESPEs of 994 CE, 775 CE, 660 BCE and 7176 BCE (panels a through d, respectively): red/blue/green/violet lines with shaded areas depict the reconstructions presented here (the median and 68% confidence intervals, respectively); orange lines with shaded areas depict the spectral reconstructions by Mekhaldi et al. (2015); greenish vertical bars represent estimates of the F_{30} fluence by Mekhaldi et al. (2021); black vertical bars in panel d correspond to the spectral estimates by Paleari et al. (2022) for the ESPE of 7176 BCE.

to negligible effect (less than a percent) on the reconstructed median value of ESPE fluences. Change of ϕ by 20% percent leads to a 2% difference for the reconstructed median value of ESPE fluence at 30 MeV, and the difference fades progressively with energy. Therefore, the proposed method is more robust to uncertainties of ϕ and M in comparison to methods used earlier, because it considers all three isotopes simultaneously and deals with absolute (not only relative) ESPE production of ^{14}C .

4 Results and discussion

4.1 Comparison with other results

Figure 1 shows the results obtained here along with earlier spectral estimates from Mekhaldi et al. (2015) for ESPEs of 994 CE and 775 CE as well as from Paleari et al. (2022) for ESPE 7176 BCE. As seen in Figure 1, the new spectral reconstruction yields significantly softer spectrum at $E > 100$ MeV than those estimated earlier by Mekhaldi et al. (2015) for ESPEs of 775 CE and 994 CE. We note that the earlier work was based

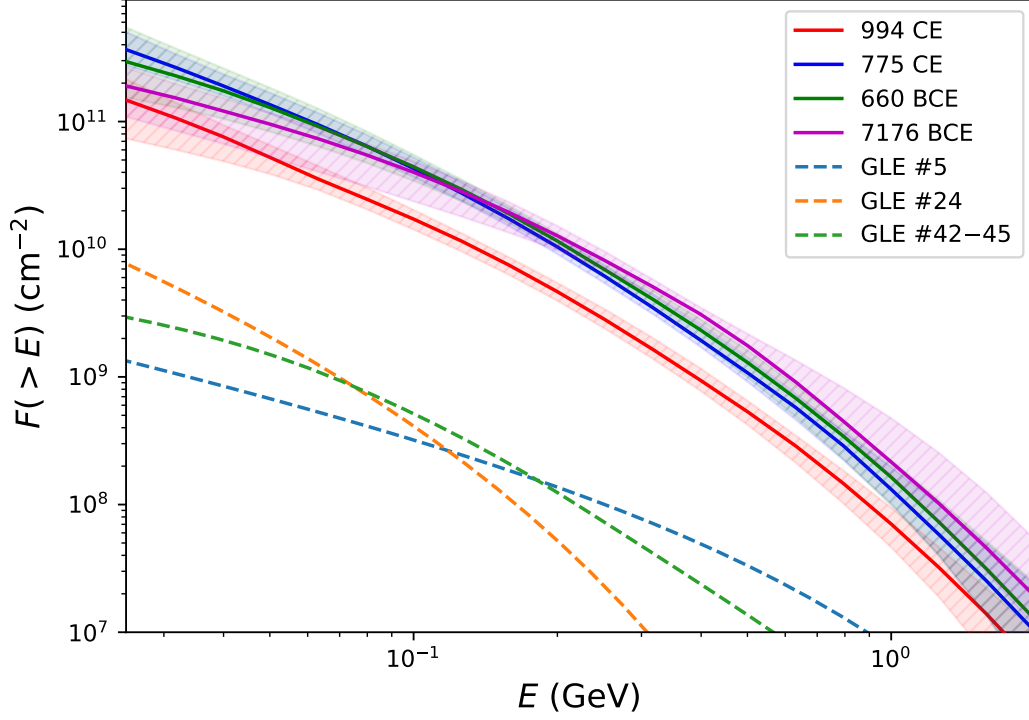


Figure 2. Integral spectral fluences of SEPs reconstructed here for the four ESPEs (solid curves with shaded areas identical to those in Figure 1). Digital data for these curves are available in Table 3. Dashed curves denote integral fluences for three selected GLEs according to Koldobskiy et al. (2021): the hard-spectrum GLE #5 (blue), soft-spectrum GLE #24 (orange) and a ‘typical’ GLE #42–45 (green), as denoted in the legend.

on a simplified assumption of a prescribed unrealistically-hard power-law shape of the SEP spectrum (Webber et al., 2007), prior to the updated fluence spectra reconstructed by Koldobskiy et al. (2021). In addition, the yield function of CI production has been essentially revisited recently (Poluianov et al., 2016). As shown previously by Mekhaldi et al. (2021), this directly transfers into a higher enhancement factor required to explain past ESPEs when comparing to modern GLEs. As such, the fluence >30 MeV of the 775 and 994 CE events were reassessed using the more realistic fluence spectra of Raukunen et al. (2018) and assuming a solar modulation function as per Steinhilber et al. (2012) and Vonmoos et al. (2006). These estimates are closer to our new reconstructed fluence spectra in comparison to the first reconstruction (Mekhaldi et al., 2015), but are still significantly lower. We examined the reason for the difference and found out that the spectral estimate by Mekhaldi et al. (2021) was based explicitly on the scaled spectrum of GLE #5 which is the hardest-spectrum known GLE. On the contrary, Paleari et al. (2022) used an ensemble of GLEs as reconstructed by Raukunen et al. (2018) resulting in a softer energy-spectrum reconstruction which is in excellent agreement with our new reconstruction (Figure 1d) based on the revised GLE spectra (Koldobskiy et al., 2021).

Figure 2 depicts integral spectra of the four ESPEs reconstructed here. As seen, three events (775 CE, 660 BCE and 7176 BCE) are very close to each other within the uncertainties, while the ESPE of 994 CE is a factor 2–3 weaker. For comparison, integral spectra of three ‘typical’ GLEs are also shown as dashed curves: the strongest hard-spectrum GLE #5 (23-Feb-1956), the strongest soft-spectrum GLE #24 (04-Aug-1972), and a ‘typical’ spectrum corresponding to a series of GLEs during Oct-Nov 1989 (GLE #42–45). One can see that the ESPE spectra are two orders of magnitude higher than that of a typical strong GLE. The fact that the CI data can be well fitted with scaled spectra of the observed GLEs implies that the physical mechanisms of acceleration and interplanetary transport of SEPs during ESPEs are similar to those of a ‘normal’ GLE, favoring the idea that ESPEs are *Black swan* (a strong unexpected event whose nature can be understood *a posteriori*, viz. once it has occurred – Taleb, 2007) rather than *Dragon king* (huge-size unexpected event whose nature cannot be understood, in the framework of the existing knowledge, even after it has occurred – Sornette & Ouillon, 2012) type events (Usoskin & Kovaltsov, 2021; Cliver et al., 2022).

4.2 Parameterization of the spectra

Different applications, for example, calculation of the cosmogenic isotope response (Eq. 5), require knowledge of not the integral flux (fluence), but differential-in-energy particle flux. For this purpose, we fitted integral spectra of ESPEs reconstructed here with the MBF spectral form (Eq. 2), which can be easily differentiated (Eq. 4). The MBF fitting procedure was based on the Monte-Carlo iterative approach. The initial guess for the MBF parameter values corresponded to GLE #5 as described in Koldobskiy et al. (2021). For each iteration, the exact values of MBF parameters ($\gamma_1, R_1, J_2, \gamma_2, R_2$) were randomly and independently chosen using the normal distribution (with σ of 10% of the parameter value). Each obtained fit parameter set was checked to be mathematically reasonable, so the fit function should not have a positive derivative anywhere, since the integral fluence cannot increase with R . This condition was quantified as $\gamma_1/R+1/R_1 > 0$ for the rigidity range $R < R_b$. For a chosen set of parameters, we have calculated expected fluence values $F_{\text{fit},i}$ using ten logarithmic bins per one order of magnitude in energy range spanning from 30 MeV to 10 GeV. After that, we assessed the agreement between fit and reconstructed ESPE fluences using χ^2 merit function:

$$\chi^2 = \sum_i \left(\frac{F_{\text{ESPE},i} - F_{\text{fit},i}}{\sigma_{\text{ESPE},i}} \right)^2 \quad (8)$$

where the summation is over bins described above, F_{ESPE} are fluence values for these energy bins, and σ_{ESPE} are corresponding 68% confidence intervals.

Table 4. Best-fit MBF (Eq. 2) parameters along with 1σ uncertainties for the ESPE fluences reconstructed here.

ESPE	γ_1	R_1 , GV	J_1 , cm^{-2}	γ_2	R_2 , GV
994 CE	$2.18^{+0.95}_{-2.78}$	$0.42^{+0.60}_{-0.32}$	$(1.25^{+1.44}_{-0.45}) \cdot 10^9$	$3.93^{+1.82}_{-0.96}$	$2.11^{+3.83}_{-1.23}$
775 CE	$1.88^{+1.06}_{-2.42}$	$0.28^{+0.49}_{-0.21}$	$(3.20^{+3.59}_{-1.28}) \cdot 10^9$	$3.70^{+2.03}_{-0.66}$	$1.44^{+2.41}_{-0.65}$
660 BCE	$1.46^{+1.31}_{-2.42}$	$0.26^{+0.41}_{-0.17}$	$(3.04^{+3.80}_{-1.17}) \cdot 10^9$	$3.90^{+1.79}_{-0.94}$	$1.94^{+3.42}_{-1.14}$
7176 BCE	$1.33^{+0.84}_{-1.89}$	$0.35^{+0.38}_{-0.22}$	$(3.51^{+5.14}_{-1.15}) \cdot 10^9$	$4.36^{+1.16}_{-1.73}$	$3.69^{+6.12}_{-2.62}$

If the value of χ_j^2 for the j th iteration appears smaller than the previous ones, it was saved as χ_{\min}^2 , the corresponding MBF parameters were considered as a new initial guess set, and the iteration counter was reset.

The procedure was repeated one million times. In addition to the best-fit values, corresponding to χ_{\min}^2 , we also calculated the 1σ uncertainty of the MBF parameters considering the parameter-value sets, for which $\chi^2 \leq \chi_{\min}^2 + 5.89$. The procedure was repeated for all GLEs MBF parameters listed in Koldobskiy et al. (2021) and minimal value of χ^2 and corresponding MBF parameters were saved. Thus obtained best-fit MBF parameters for ESPE fluence fitting together with 68% c.i. uncertainties are given in Table 4. MBF parameters are interrelated, the example of their mutual distributions and also the dependence of χ^2 for best-fit (red dot) and 68% c.i. interval (blue dots) is shown in Figure 3 for the event 775 CE. Other ESPEs demonstrate similar parameter interrelation and quality of the fit.

4.3 Expected NM response to ESPE

We also investigated quantitatively the possible NM response to an ESPE should it occur now under the single event hypothesis. The strength of a GLE event can be quantified with the integral relative increase I , measured in %-hours, of a sea-level polar NM count rate caused by SEPs above the GCR background (Asvestari et al., 2017; Usoskin, Koldobskiy, Kovaltsov, Gil, et al., 2020). The greatest known integral increase of NM count rate of 5300 %*h was registered during GLE #5 by Ottawa NM (subpolar sea-level NM). We have calculated NM integral increase due to ESPEs using the yield function approach (Eq. 5) utilizing the NM yield function calculated by Mishev et al. (2020). For assessment of GCR background we took LIS by Vos and Potgieter (2015), consideration of heavy elements from Koldobskiy et al. (2019) and solar modulation potential values from Table 1. Three events of similarly high magnitude (775 CE, 660 BCE, and 7176 BCE) were taken as reference events. We took MBF fit parameter realizations within 68 % c.i. for each of considered events and calculated the expected NM response to these events for a polar sea-level NM (geomagnetic cutoff rigidity $P_c=0$ GV, atmospheric depth $h=1000$ g/cm²). The estimated integral increase I was found in the range from ~ 75000 to ~ 280000 %*h, which is a factor $\sim 15-50$ greater than GLE #5. Such a strong enhancement of the count rate (a typical count rate of a NM64 is about 10 counts/sec/counter) would likely causes a saturation of a real NM considering the standard dead-time of the standard NM read-out electronics of 2 milliseconds.

5 Conclusions

A new quantitative non-parametric multi-proxy method of the reconstruction of integral fluences is presented as based on the scaling of the existing GLE spectra to match all the available cosmogenic-isotope data for each event. This allowed us to consistently reconstruct integral fluxes of all four extreme solar particle events for which all three CIs

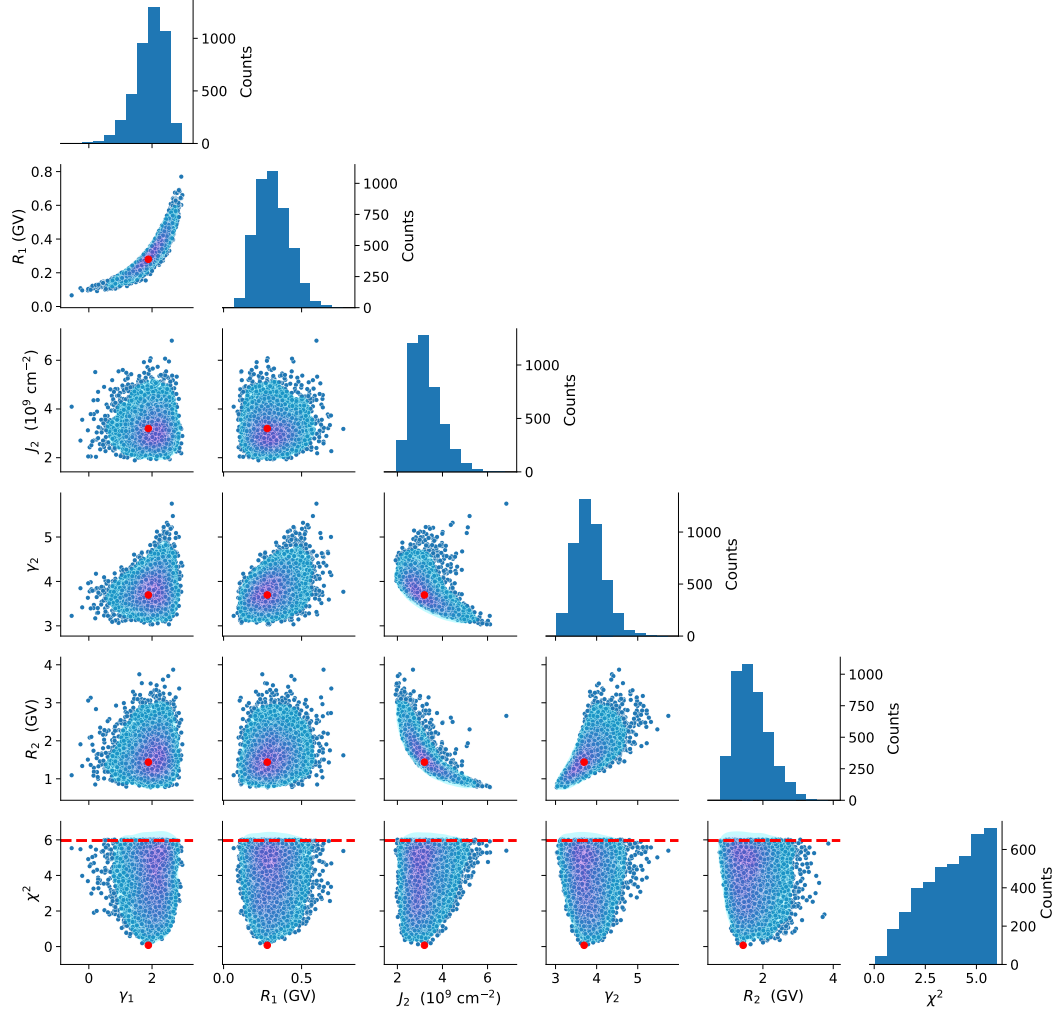


Figure 3. Interrelation of MBF parameters and their dependence on χ^2 for ESPE 775 CE. Red dot corresponds to best-fit solution, other points are within 68% c.i.

are currently measured. The method utilizes a Monte Carlo approach to find the most probable solution in the form of the scaled directly observed GLE spectra and to estimate the uncertainties. The combination of the newly revisited, more robust GLE spectra estimates (Koldobskiy et al., 2021) and an updated CI production function (Poluianov et al., 2016) used for the reconstruction yielded an order-of-magnitude higher fluence of lower energy <100 MeV relative to the original estimates for the 994 CE, 775 CE, and 660 BCE ESPEs. The result obtained here for EPSE 7176 BCE is in good agreement with the recent reconstruction by Paleari et al. (2022).

SEPs with energies $E < 100$ MeV are most dangerous for technological and health hazards (e.g., Miyake et al., 2019) so new ESPE fluence reconstructions allows a better assessment of the potential impact of ESPE on modern society.

Statistically justified opportunity to describe ESPE integral flux with scaled spectra of typical strong GLE events recorded during the recent decades implies that ESPEs are likely produced by a mechanism similar to that of the ‘regular’ GLEs. This suggests that ESPE are likely *Black-swan* events whose origin can be understood in terms of the existing knowledge (Usoskin & Kovaltsov, 2021; Cliver et al., 2022).

The spectral shape of the four analyzed events appear similar to one another. Interestingly, while the event of 994 CE is somewhat smaller, the other three ESPEs have very similar intensities. Since it is unlikely that significantly stronger ESPEs could be found over the Holocene (Miyake et al., 2019; Cliver et al., 2022), this could be speculated as an upper limit of the SEP events produced by the Sun. However, more data including the detection of new ESPEs, confirmation of existing candidates and their fluence reconstructions are required to prove that.

In conclusion, a new method, based on cosmogenic-isotope proxy, for the robust non-parametric reconstruction of integral energy spectra for ESPE has been proposed and applied to four ESPEs detected over the last millennia, viz. 7176 BCE, 660 BCE, 775 CE, and 994 CE. The reconstructed ESPE spectral fluences have been parameterized in the form of the modified Band function. This result provides new insight into the physics of rare extreme solar events on the multi-millennial timescale.

Data Availability Statement

Datasets used for ESPE reconstructions are available elsewhere. ESPE fluences with fine energy resolution are available in the Supplementary Material to this paper.

Acknowledgments

This work was partly supported by the Academy of Finland (Projects ESPERA no. 321882 and QUASARE no. 330064), University of Oulu (Project SARPEDON). F. Mekhaldi acknowledges funding from the Swedish Research Council (no. 2020-00420), and the Royal Physiographic Society of Lund. The ISSI Team #510 (*Solar Extreme Events: Setting up a Paradigm*, led by F. Miyake and I. Usoskin) is acknowledged for stimulating discussions. Research was performed using NumPy (Harris et al., 2020), SciPy (Virtanen et al., 2020), pandas (Pandas development team, 2020) and matplotlib (Hunter, 2007) open-source Python packages.

References

Asvestari, E., Gil, A., Kovaltsov, G. A., & Usoskin, I. G. (2017). Neutron Monitors and Cosmogenic Isotopes as Cosmic Ray Energy-Integration Detectors: Effective Yield Functions, Effective Energy, and Its Dependence on the Local Interstellar Spectrum. *J. Geophys. Res. (Space Phys.)*, 122, 9790-9802. doi:

- 10.1002/2017JA024469
- Asvestari, E., Willamo, T., Gil, A., Usoskin, I. G., Kovaltsov, G. A., Mikhailov, V. V., & Mayorov, A. (2017). Analysis of Ground Level Enhancements (GLE): Extreme solar energetic particle events have hard spectra. *Adv. Sp. Res.*, 60(4), 781–787. Retrieved from <https://linkinghub.elsevier.com/retrieve/pii/S0273117716304963> doi: 10.1016/j.asr.2016.08.043
- Bard, E., Raisbeck, G., Yiou, F., & Jouzel, J. (2000). Solar irradiance during the last 1200 years based on cosmogenic nuclides. *Tellus, Ser. B Chem. Phys. Meteorol.*, 52(3), 985–992. doi: 10.1034/j.1600-0889.2000.d01-7.x
- Beer, J., McCracken, K., & von Steiger, R. (2012). *Cosmogenic radionuclides: Theory and applications in the terrestrial and space environments*. Berlin: Springer.
- Brehm, N., Bayliss, A., Christl, M., Synal, H.-A., Adolphi, F., Beer, J., ... Wacker, L. (2021, jan). Eleven-year solar cycles over the last millennium revealed by radiocarbon in tree rings. *Nat. Geosci.*, 14(1), 10–15. Retrieved from <http://www.nature.com/articles/s41561-020-00674-0> doi: 10.1038/s41561-020-00674-0
- Brehm, N., Christl, M., Knowles, T. D. J., Casanova, E., Evershed, R. P., Adolphi, F., ... Wacker, L. (2022). Tree-rings reveal two strong solar proton events in 7176 and 5259 BCE. *Nat. Commun.*, 13(1), 1196. Retrieved from <https://www.nature.com/articles/s41467-022-28804-9> doi: 10.1038/s41467-022-28804-9
- Büntgen, U., Wacker, L., Galván, J. D., Arnold, S., Arseneault, D., Baillie, M., ... Young, G. H. (2018). Tree rings reveal globally coherent signature of cosmogenic radiocarbon events in 774 and 993 CE. *Nat. Commun.*, 9(1), 1–7. doi: 10.1038/s41467-018-06036-0
- Caballero-Lopez, R., & Moraal, H. (2004). Limitations of the force field equation to describe cosmic ray modulation. *J. Geophys. Res.*, 109, A01101. doi: 10.1029/2003JA010098
- Cliver, E. W., Schrijver, C. J., Shibata, K., & Usoskin, I. (2022). Extreme solar events. *Liv. Rev. Solar Phys.*, 19(1), 2. doi: 10.1007/s41116-022-00033-8
- Desai, M., & Giacalone, J. (2016). Large gradual solar energetic particle events. *Liv. Rev. Solar Phys.*, 13, 3. doi: 10.1007/s41116-016-0002-5
- Field, C., Schmidt, G., Koch, D., & Salyk, C. (2006). Modeling production and climate-related impacts on ^{10}Be concentration in ice cores. *J. Geophys. Res.*, 111, D15107.
- Golubenkov, K., Rozanov, E., Kovaltsov, G., Leppänen, A.-P., Sukhodolov, T., & Usoskin, I. (2021). Application of CCM SOCOL-AERv2-BE to cosmogenic beryllium isotopes: description and validation for polar regions. *Geosci. Model Dev.*, 14(12), 7605–7620. doi: 10.5194/gmd-14-7605-2021
- Harris, C. R., Millman, K. J., van der Walt, S. J., Gommers, R., Virtanen, P., Cournapeau, D., ... Oliphant, T. E. (2020, sep). Array programming with NumPy. *Nature*, 585(7825), 357–362. Retrieved from <https://doi.org/10.1038/s41586-020-2649-2> doi: 10.1038/s41586-020-2649-2
- Heikkilä, U., Beer, J., Abreu, J. A., & Steinhilber, F. (2013). On the Atmospheric Transport and Deposition of the Cosmogenic Radionuclides (^{10}Be): A Review. *Space Sci. Rev.*, 176, 321–332. doi: 10.1007/s11214-011-9838-0
- Heikkilä, U., Beer, J., & Feichter, J. (2009). Meridional transport and deposition of atmospheric ^{10}Be . *Atmos. Chem. Phys.*, 9(2), 515–527. doi: 10.5194/acp-9-515-2009
- Herbst, K., Kopp, A., Heber, B., Steinhilber, F., Fichtner, H., Scherer, K., & Matthiä, D. (2010). On the importance of the local interstellar spectrum for the solar modulation parameter. *J. Geophys. Res.*, 115, D00I20. doi: 10.1029/2009JD012557

- Hunter, J. D. (2007). Matplotlib: A 2D Graphics Environment. *Comput. Sci. Eng.*, 9(3), 90–95. Retrieved from <http://ieeexplore.ieee.org/document/4160265/> doi: 10.1109/MCSE.2007.55
- Knudsen, M. F., Riisager, P., Donadini, F., Snowball, I., Muscheler, R., Korhonen, K., & Pesonen, L. J. (2008, jul). Variations in the geomagnetic dipole moment during the Holocene and the past 50 kyr. *Earth Planet. Sci. Lett.*, 272(1-2), 319–329. Retrieved from <https://linkinghub.elsevier.com/retrieve/pii/S0012821X08003154> doi: 10.1016/j.epsl.2008.04.048
- Koldobskiy, S. A., Bindi, V., Corti, C., Kovaltsov, G. A., & Usoskin, I. G. (2019). Validation of the neutron monitor yield function using data from AMS-02 experiment, 2011–2017. *J. Geophys. Res. Sp. Phys.*, 124(4), 2367–2379. Retrieved from <https://onlinelibrary.wiley.com/doi/abs/10.1029/2018JA026340><http://arxiv.org/abs/1904.01929><http://dx.doi.org/10.1029/2018JA026340> doi: 10.1029/2018JA026340
- Koldobskiy, S. A., Raukunen, O., Vainio, R., Kovaltsov, G. A., & Usoskin, I. (2021). New reconstruction of event-integrated spectra (spectral fluences) for major solar energetic particle events. *Astron. Astrophys.*, 647, A132. Retrieved from <https://www.aanda.org/10.1051/0004-6361/202040058> doi: 10.1051/0004-6361/202040058
- Koldobskiy, S. A., Usoskin, I., & Kovaltsov, G. A. (2022). Effective Energy of Cosmogenic Isotope (^{10}Be , ^{14}C and ^{36}Cl) Production by Solar Energetic Particles and Galactic Cosmic Rays. *J. Geophys. Res. Sp. Phys.*, 127(1), 1–13. Retrieved from <https://onlinelibrary.wiley.com/doi/10.1029/2021JA029919> doi: 10.1029/2021JA029919
- Kovaltsov, G., Mishev, A., & Usoskin, I. (2012). A new model of cosmogenic production of radiocarbon ^{14}C in the atmosphere. *Earth Planet. Sci. Lett.*, 337, 114–120. doi: 10.1016/j.epsl.2012.05.036
- Mekhaldi, F., Adolphi, F., Herbst, K., & Muscheler, R. (2021). The Signal of Solar Storms Embedded in Cosmogenic Radionuclides: Detectability and Uncertainties. *J. Geophys. Res. Sp. Phys.*, 126(8). doi: 10.1029/2021JA029351
- Mekhaldi, F., Muscheler, R., Adolphi, F., Aldahan, A., Beer, J., McConnell, J. R., ... Woodruff, T. E. (2015). Multiradionuclide evidence for the solar origin of the cosmic-ray events of AD 774/5 and 993/4. *Nat. Commun.*, 6(1), 8611. doi: 10.1038/ncomms9611
- Mishev, A. L., Koldobskiy, S. A., Kovaltsov, G. A., Gil, A., & Usoskin, I. G. (2020, feb). Updated Neutron-Monitor Yield Function: Bridging Between In Situ and Ground-Based Cosmic Ray Measurements. *J. Geophys. Res. Sp. Phys.*, 125(2), e2019JA027433. Retrieved from <https://onlinelibrary.wiley.com/doi/abs/10.1029/2019JA027433> doi: 10.1029/2019JA027433
- Miyake, F., Masuda, K., & Nakamura, T. (2013). Another rapid event in the carbon-14 content of tree rings. *Nature Comm.*, 4, 1748. doi: 10.1038/ncomms2783
- Miyake, F., Nagaya, K., Masuda, K., & Nakamura, T. (2012). A signature of cosmic-ray increase in ad 774–775 from tree rings in Japan. *Nature*, 486(7402), 240–242. Retrieved from <http://dx.doi.org/10.1038/nature11123> doi: 10.1038/nature11123
- Miyake, F., Panyushkina, I. P., Jull, A. J. T., Adolphi, F., Brehm, N., Helama, S., ... Wacker, L. (2021). A single year cosmic ray event at 5410 BCE registered in ^{14}C of tree rings. *Geophys. Res. Lett.*, 48, e2021GL093419. doi: 10.1029/2021GL093419
- Miyake, F., Usoskin, I., & Poluianov, S. (Eds.). (2019). *Extreme solar particle storms: The hostile sun*. Bristol, UK: IOP Publishing. doi: 10.1088/2514-3433/ab404a
- Muscheler, R., Joos, F., Beer, J., Müller, S. A., Vonmoos, M., & Snowball, I. (2007). Solar activity during the last 1000 yr inferred from radionuclide records. *Quat.*

- Sci. Rev.*, 26(1-2), 82–97. doi: 10.1016/j.quascirev.2006.07.012
- Nevalainen, J., Usoskin, I. G., & Mishev, A. (2013). Eccentric dipole approximation of the geomagnetic field: Application to cosmic ray computations. *Adv. Space Res.*, 52, 22–29. doi: 10.1016/j.asr.2013.02.020
- O’Hare, P., Mekhaldi, F., Adolphi, F., Raisbeck, G., Aldahan, A., Anderberg, E., ... Muscheler, R. (2019). Multiradionuclide evidence for an extreme solar proton event around 2,610 B.P. (~660 BC). *Proc. Natl. Acad. Sci. U. S. A.*, 116(13), 5961–5966. doi: 10.1073/pnas.1815725116
- Paleari, C. I., Mekhaldi, F., Adolphi, F., Christl, M., Vockenhuber, C., Gautschi, P., ... Muscheler, R. (2022). Cosmogenic radionuclides reveal an extreme solar particle storm near a solar minimum 9125 years BP. *Nat. Commun.*, 13(1), 214. Retrieved from <https://www.nature.com/articles/s41467-021-27891-4> doi: 10.1038/s41467-021-27891-4
- Pandas development team, T. (2020, feb). *pandas-dev/pandas: Pandas*. Zenodo. Retrieved from <https://doi.org/10.5281/zenodo.3509134> doi: 10.5281/zenodo.3509134
- Panovska, S., Constable, C. G., & Korte, M. (2018, dec). Extending Global Continuous Geomagnetic Field Reconstructions on Timescales Beyond Human Civilization. *Geochemistry, Geophys. Geosystems*, 19(12), 4757–4772. Retrieved from <https://onlinelibrary.wiley.com/doi/10.1029/2018GC007966> doi: 10.1029/2018GC007966
- Park, J., Southon, J., Fahrni, S., Creasman, P. P., & Mewaldt, R. (2017). Relationship between solar activity and ^{14}C peaks in AD 775, AD 994, and 660 BC. *Radiocarbon*, 59, 1147–1156.
- Pedro, J., van Ommen, T., Curran, M., Morgan, V., Smith, A., & McMorro, A. (2006). Evidence for climate modulation of the ^{10}Be solar activity proxy. *J. Geophys. Res. Atmos.*, 111(21), 1–6. doi: 10.1029/2005JD006764
- Poluianov, S. V., Kovaltsov, G. A., Mishev, A. L., & Usoskin, I. G. (2016). Production of cosmogenic isotopes ^7Be , ^{10}Be , ^{14}C , ^{22}Na , and ^{36}Cl in the atmosphere: Altitudinal profiles of yield functions. *J. Geophys. Res. Atmos.*, 121(13), 8125–8136. doi: 10.1002/2016JD025034
- Press, W. H., Teukolsky, S. A., Vetterling, W. T., & Flannery, B. P. (2007). *Numerical Recipes 3rd Edition: The Art of Scientific Computing* (3rd ed.). Cambridge University Press.
- Raukunen, O., Vainio, R., Tylka, A. J., Dietrich, W. F., Jiggins, P., Heynderickx, D., ... Siipola, R. (2018, jan). Two solar proton fluence models based on ground level enhancement observations. *J. Sp. Weather Sp. Clim.*, 8, A04. Retrieved from <https://www.swsc-journal.org/articles/swsc/pdf/2018/01/swsc170071.pdf> <https://www.swsc-journal.org/10.1051/swsc/2017031> doi: 10.1051/swsc/2017031
- Sakurai, H., Tokanai, F., Miyake, F., Horiuchi, K., Masuda, K., Miyahara, H., ... Moriya, T. (2020). Prolonged production of ^{14}C during the ~660 BCE solar proton event from Japanese tree rings. *Sci. Rep.*, 10(1), 1–7. doi: 10.1038/s41598-019-57273-2
- Solanki, S. K., Usoskin, I. G., Kromer, B., Schüssler, M., & Beer, J. (2004). Unusual activity of the Sun during recent decades compared to the previous 11,000 years. *Nature*, 431(7012), 1084–1087. doi: 10.1038/nature02995
- Sornette, D., & Ouillon, G. (2012). Dragon-kings: Mechanisms, statistical methods and empirical evidence. *Europ. Phys. J. Spec. Top.*, 205. doi: 10.1140/epjst/e2012-01559-5
- Steinilber, F., Abreu, J., Beer, J., Brunner, I., Christl, M., Fischer, H., ... Wilhelm, F. (2012). 9,400 years of cosmic radiation and solar activity from ice cores and tree rings. *Proc. Nat. Acad. Sci. USA*, 109(16), 5967–5971. doi: 10.1073/pnas.1118965109
- Sukhodolov, T., Usoskin, I., Rozanov, E., Asvestari, E., Ball, W. T., Curran, M. A.,

- ... Traversi, R. (2017). Atmospheric impacts of the strongest known solar particle storm of 775 AD. *Sci. Rep.*, 7, 1–9. doi: 10.1038/srep45257
- Synal, H.-A., & Wacker, L. (2010). AMS measurement technique after 30 years: Possibilities and limitations of low energy systems. *Nuc. Instrum. Meth. Phys. Res. B*, 268(7-8), 701-707. doi: 10.1016/j.nimb.2009.10.009
- Taleb, N. (2007). *The Black Swan: the impact of the highly improbable*. New York: Random House.
- Usoskin, I. (2017). A History of Solar Activity over Millennia. *Living Rev. Solar Phys.*, 14, 3. doi: 10.1007/s41116-017-0006-9
- Usoskin, I., Alanko-Huotari, K., Kovaltsov, G. A., & Mursula, K. (2005). Heliospheric modulation of cosmic rays: Monthly reconstruction for 1951–2004. *J. Geophys. Res.*, 110, A12108. doi: 10.1029/2005JA011250
- Usoskin, I., Koldobskiy, S., Kovaltsov, G., Gil, A., Usoskina, I., Willamo, T., & Ibragimov, A. (2020). Revised GLE database: Fluences of solar energetic particles as measured by the neutron-monitor network since 1956. *Astron. Astrophys.*, 640, A17. Retrieved from <https://www.aanda.org/10.1051/0004-6361/202038272> doi: 10.1051/0004-6361/202038272
- Usoskin, I., Koldobskiy, S., Kovaltsov, G., Rozanov, E., Sukhodolov, T., Mishev, A., & Mironova, I. (2020). Revisited reference solar proton event of 23-Feb-1956: Assessment of the cosmogenic-isotope method sensitivity to extreme solar events. *J. Geophys. Res. Sp. Phys.*, 125(6), e2020JA027921. Retrieved from <https://onlinelibrary.wiley.com/doi/abs/10.1029/2020JA027921><http://arxiv.org/abs/2005.10597><http://dx.doi.org/10.1029/2020JA027921> doi: 10.1029/2020JA027921
- Usoskin, I., & Kovaltsov, G. (2021). Mind the Gap: New Precise 14 C Data Indicate the Nature of Extreme Solar Particle Events. *Geophys. Res. Lett.*, 48(17), 1–5. Retrieved from <https://onlinelibrary.wiley.com/doi/10.1029/2021GL094848> doi: 10.1029/2021GL094848
- Usoskin, I., Kromer, B., Ludlow, F., Beer, J., Friedrich, M., Kovaltsov, G. A., ... Wacker, L. (2013). The AD775 cosmic event revisited: the Sun is to blame. *Astron. Astrophys.*, 552, L3. doi: 10.1051/0004-6361/201321080
- Usoskin, I., Solanki, S., Kovaltsov, G., Beer, J., & Kromer, B. (2006). Solar proton events in cosmogenic isotope data. *Geophys. Res. Lett.*, 33, L08107. doi: 10.1029/2006GL026059
- Usoskin, I., Solanki, S. K., & Korte, M. (2006). Solar activity reconstructed over the last 7000 years: The influence of geomagnetic field changes. *Geophys. Res. Lett.*, 33, 8103. doi: 10.1029/2006GL025921
- Usoskin, I., Solanki, S. K., Krivova, N. A., Hofer, B., Kovaltsov, G. A., Wacker, L., ... Kromer, B. (2021). Solar cyclic activity over the last millennium reconstructed from annual 14C data. *Astron. Astrophys.*, 649, 1–13. doi: 10.1051/0004-6361/202140711
- Usoskin, I. G., Horiuchi, K., Solanki, S., Kovaltsov, G. A., & Bard, E. (2009). On the common solar signal in different cosmogenic isotope data sets. *J. Geophys. Res.*, 114(A13), A03112. doi: 10.1029/2008JA013888
- Vainio, R., Valtonen, E., Heber, B., Malandraki, O. E., Papaioannou, A., Klein, K.-L., ... Vilmer, N. (2013). The first SEPServer event catalogue ~68-MeV solar proton events observed at 1 AU in 1996–2010. *J. Space Weather Space Climate*, 3, A12. doi: 10.1051/swsc/2013030
- Virtanen, P., Gommers, R., Oliphant, T. E., Haberland, M., Reddy, T., Cournapeau, D., ... Vázquez-Baeza, Y. (2020, mar). SciPy 1.0: fundamental algorithms for scientific computing in Python. *Nat. Methods*, 17(3), 261–272. Retrieved from <https://www.nature.com/articles/s41592-019-0686-2> doi: 10.1038/s41592-019-0686-2
- Vonmoos, M., Beer, J., & Muscheler, R. (2006). Large variations in Holocene solar activity: Constraints from ^{10}Be in the Greenland Ice Core Project ice core. *J.*

593 *Geophys. Res. Sp. Phys.*, *111*(10), 1–14. doi: 10.1029/2005JA011500
594 Vos, E. E., & Potgieter, M. S. (2015). New modeling of galactic proton modulation
595 during the minimum of solar cycle 23/24. *Astrophys. J.*, *815*(2), 119. Retrieved
596 from [http://stacks.iop.org/0004-637X/815/i=2/a=119?key=crossref](http://stacks.iop.org/0004-637X/815/i=2/a=119?key=crossref.c12615a9ee5e7e958d199cb500017eee)
597 [.c12615a9ee5e7e958d199cb500017eee](http://stacks.iop.org/0004-637X/815/i=2/a=119?key=crossref.c12615a9ee5e7e958d199cb500017eee) doi: 10.1088/0004-637X/815/2/119
598 Webber, W., Higbie, P., & McCracken, K. (2007). Production of the cosmogenic iso-
599 topes ^3H , ^7Be , ^{10}Be , and ^{36}Cl in the Earth’s atmosphere by solar and galactic
600 cosmic rays. *J. Geophys. Res.*, *112*, A10106. doi: 10.1029/2007JA012499
601 Wu, C. J., Usoskin, I. G., Krivova, N., Kovaltsov, G. A., Baroni, M., Bard, E.,
602 & Solanki, S. K. (2018). Solar activity over nine millennia: A consistent
603 multi-proxy reconstruction. *Astron. Astrophys.*, *615*, 93. Retrieved from
604 <https://doi.org/10.1051/0004-6361/201731892> doi: 10.1051/0004-6361/
605 201731892
606 Zheng, M., Adolphi, F., Sjolte, J., Aldahan, A., Possnert, G., Wu, M., ...
607 Muscheler, R. (2020). Solar and climate signals revealed by seasonal ^{10}Be
608 data from the NEEM ice core project for the neutron monitor period. *Earth*
609 *Planet. Sci. Lett.*, *541*, 116273. Retrieved from [https://doi.org/10.1016/](https://doi.org/10.1016/j.epsl.2020.116273)
610 [j.epsl.2020.116273](https://doi.org/10.1016/j.epsl.2020.116273) doi: 10.1016/j.epsl.2020.116273